SUPPLEMENTARY MATERIALS

List of Abbreviations

3-PEHPC	3-(3-pyridyl)-2-hydroxy-2-phosphono propanoic acid
4E-BP1	4E-binding protein 1
AAV	adeno-associated virus
Ac-STAT3	acetylated STAT3
ADP	adenosine diphosphate
ADPR	ADP ribose
AKT1	protein kinase B
ANA	antinuclear antibodies
cADPR	cyclic ADPR
CBA	cytometric bead array
CRISPR	clustered regularly interspaced short palindromic repeats
cRPMI	complete RPMI 1640 medium
DN	double negative
FOXO1	forkhead box O1
GFP	green fluorescent protein
HRES-1	human T lymphotropic virus type I-related endogenous retroviral sequence
IFN	interferon
IL	interleukin
IRES	internal ribosomal entry site
KO	knockout
LC-MS/MS	liquid chromatography tandem mass spectrometry
LTR	LysoTracker red
MFI	mean fluorescence intensity
mTOR	mechanistic target of rapamycin
mTORC	mTOR complex
NAD^+	nicotinamide adenine dinucleotide
PBMC	peripheral blood mononuclear cells
PBS	phosphate-buffered saline
PMA	phorbol 12-myristate 13-acetate
pSTAT3	phosphorylated STAT3
$Rab4A^+$	Rab4A-overexpressing
$Rab4A^{DN}$	Rab4A-dominant negative
S6RP	S6 ribosomal protein
SEM	standard error of the mean
SLE	systemic lupus erythematosus
STAT3	signal transducer and activator of transcription 3
TC	triple congenic
TCA	tricarboxylic acid
TCR	T cell receptor
T_H	T helper cell
TNF	tumor necrosis factor
T_{reg}	regulatory T cell
UMAP	uniform manifold approximation and projection for dimension reduction

Supplementary Table S1. Flow cytometry antibodies

Surface Antibodies

Marker	Fluorochrome	Target	Vendor	Catalog	Dilution
CD14	Spark Blue 550	Human	Biolegend	367148	1:100
CD11c	Alexa Fluor 532	Human	Novus Biologicals	NB100-2711AF532	1:100
CD8	PerCP	Human	BD Biosciences	347314	1:50
CD209	PerCP-Cy5.5	Human	Biolegend	330110	1:100
CD51/CD61	APC	Human	Biolegend	304416	1:100
CD95	APC-Cy7	Human	Biolegend	305636	1:100
CD38	APC-Fire 810	Human	Biolegend	303550	1:100
CD98	BUV615	Human	BD Biosciences	751522	1:100
CD123	BUV661	Human	BD Biosciences	751838	1:100
IgD	BUV737	Human	BD Biosciences	612798	1:100
CD45RO	BUV805	Human	BD Biosciences	748367	1:100
CD45RA	BUV395	Human	BD Biosciences	740298	1:100
CD24	Alexa Fluor 350	Human	Novus Biologicals	NB100-77903AF350	1:100
CD27	BUV496	Human	BD Biosciences	741145	1:100
CD25	BUV563	Human	BD Biosciences	741365	1:100
CD138	BV605	Human	Biolegend	356520	1:100
CD71	BV650	Human	Biolegend	334116	1:100
PD-1	BV750	Human	BD Biosciences	747446	1:100
CD19	V450	Human	BD Biosciences	560353	1:100
CD62L	BV480	Human	BD Biosciences	566111	1:100
CD3	BV510	Human	BD Biosciences	564713	1:100
CD4	BV570	Human	Biolegend	300534	1:100
CD47	PE	Human	Biolegend	323108	1:100
CD56	PE-Cy5	Human	Biolegend	362516	1:100
CCR7	PE-Cy7	Human	Biolegend	353226	1:100
CD3	BV711	Mouse	BD Biosciences	563123	1:50
CD4	PerCP-Cy5.5	Mouse	Biolegend	100434	1:50
CD8	APC-Cy7	Mouse	Biolegend	100714	1:50
CD19	APC-R700	Mouse	BD Biosciences	565473	1:50
CD38	BV786	Mouse	BD Biosciences	740887	1:50

Intracellular Antibodies

Marker	Fluorochrome	Target	Vendor	Catalog	Dilution
IL-6	APC	Human	Biolegend	501112	1:50
IL-21	Alexa Fluor 647	Human	Biolegend	513006	1:50
IFNγ	Alexa Fluor 700	Human	BD Biosciences	557995	1:100
IL-4	BV421	Human	BD Biosciences	562986	1:50
TNFα	BV711	Human	Biolegend	502940	1:50
IL-17A	PE	Human	BD Biosciences	560436	1:25
IL-2	DyLight 550	Human	Novus Biologicals	NBP2-90004R	1:50
IL-10	PE-CF594	Human	BD Biosciences	562400	1:50
Bcl-6	PerCP-eFluor 710	Human	ThermoFisher Scientific	46-9880-42	1:50
pS6RP (S235/236)	Alexa Fluor 647	Human	Cell Signaling Technology	48515	1:100
GLUT-1	Alexa Fluor 700	Human	R&D Systems	FAB1418N	1:50
FoxP3	BV421	Human	Biolegend	320124	1:50
T-bet	BV711	Human	BD Biosciences	563320	1:50
CTLA-4	BV785	Human	Biolegend	369624	1:50
GLUT-4	Alexa Fluor 405	Human	R&D Systems	FAB86541V	1:50
GATA-3	DyLight 550	Human	Novus Biologicals	NBP2-70796R	1:50
pAkt1 (S473)	PE-CF594	Human	BD Biosciences	562465	1:50
p4EBP1 (T37/46)	PE-Cy7	Human	Cell Signaling Technology	45613S	1:50

Supplementary Table S2. Western blot antibodies

Primary Antibodies

Marker	Molecular Weight (kDa)	Host	Target	Vendor	Catalog	Dilution
CD38	34-45	Rabbit	Human	Abcam	ab108403	1:2000
Rab4	24-25	Rabbit	Human, mouse	Abcam	ab108974	1:2000
Actin	42	Mouse	All vertebrates	EMD Millipore	MAB1501R	1:10000
CD4	55	Rabbit	Human, mouse	Santa Cruz	sc-7219	1:500
Acetyl-STAT3 (K685)	79, 86	Rabbit	Human	Cell Signaling Technology	2523L	1:500
pSTAT3 (S727)	86	Rabbit	Human, mouse	Cell Signaling Technology	9134S	1:1000
STAT3	79-86	Rabbit	Human, mouse	Cell Signaling Technology	12640S	1:1000
FOXO1	78-82	Rabbit	Human, mouse	Cell Signaling Technology	2880T	1:1000

Secondary Antibodies

Target	Host	Conjugate	Vendor	Catalog	Dilution
Rabbit	Donkey	HRP	Fisher Scientific	45-000-683	1:5000
Mouse	Goat	HRP	Jackson Immuno Research	115-035-146	1:5000

Supplementary Table S3. Demographics of healthy donors for AAV infection

Age (Years)	Sex	Race	Frequency
22	F	White/Not Hispanic	1
24	F	White/Not Hispanic	1
25	F	White/Not Hispanic	1
34	F	White/Not Hispanic	3
43	F	White/Not Hispanic	2
47	F	White/Not Hispanic	1
48	F	White/Not Hispanic	2
51	F	White/Not Hispanic	2
57	M	White/Not Hispanic	1
63	F/M	White/Not Hispanic	3 (2F, 1M)

Total donors: 18 (16 Female, 2 Male)

Supplementary Table S4. Demographics of SLE patients and matched controls

SLE Patients

Pair Number	ID	Age (Years)	Sex	Race
1	01-014-01	55	F	White/Not Hispanic
2	01-015-01	54	F	White/Not Hispanic
3	01-018-01	66	F	White/Not Hispanic
4	01-021-01	68	F	White/Not Hispanic
5	01-022-01	40	F	White/Not Hispanic
6	01-023-01	49	F	White/Not Hispanic
7	01-024-01	68	F	White/Not Hispanic
8	01-026-01	55	F	White/Not Hispanic
9	01-027-01	56	F	White/Not Hispanic
10	01-028-01	42	F	White/Not Hispanic
11	01-029-01	65	F	White/Not Hispanic
12	01-030-01	26	F	White/Not Hispanic
13	01-031-01	33	F	White/Not Hispanic
14	01-032-01	35	F	White/Not Hispanic
15	01-033-01	33	F	White/Not Hispanic
16	01-034-01	42	F	White/Not Hispanic
17	01-035-01	49	F	American Indian or Alaska Native/Not Hispanic
18	01-036-01	31	F	White/Not Hispanic
19	01-037-01	56	F	White/Not Hispanic
20	01-039-01	54	F	White/Not Hispanic
21	01-040-01	44	F	White/Not Hispanic
22	01-042-01	51	F	Black/Not Hispanic
23	01-043-01	42	F	White/Not Hispanic
24	01-046-01	43	F	White/Not Hispanic

Healthy Donors

Pair Number	ID	Age (Years)	Sex	Race
1	C-01-004-02	43	F	White/Not Hispanic
2, 3	C-01-006-01	61	F	White/Not Hispanic
4	C-01-007-01	60	F	White/Not Hispanic
5	C-01-009-01	33	F	White/Not Hispanic
6	C-01-010-01	52	F	White/Not Hispanic
7, 8	C-01-008-01	60	F	White/Not Hispanic
9	C-01-015-01	52	F	White/Not Hispanic
10	C-01-004-03	43	F	White/Not Hispanic
11	C-01-011-01	63	F	White/Not Hispanic
12	C-01-012-01	32	F	White/Not Hispanic
13	C-01-014-01	36	F	White/Not Hispanic
14, 15	C-01-018-01	41	F	White/Not Hispanic
16	C-01-019-01	39	F	White/Not Hispanic
17	C-01-001-03	39	F	White/Not Hispanic

18	C-01-020-01	24	F	White/Not Hispanic
19	C-01-010-02	57	F	White/Not Hispanic
20	C-01-021-01	57	F	White/Not Hispanic
21	C-01-014-02	37	F	White/Not Hispanic
22	C-01-019-02	39	F	White/Not Hispanic
23	C-01-004-04	43	F	White/Not Hispanic
24	C-01-023-01	50	F	White/Not Hispanic

Supplementary Table S5. Targeted detection of metabolites by LC-MS/MS.

Name	Abbreviation	KEGG	HMDB	Molecular formula	Exact mass (negative mode)	Exact mass (positive mode)
Nicotinamide adenine dinucleotide	NAD^+	C00003	HMDB0000902	$C_{21}H_{28}N_7O_{14}P_2$	662.1018	664.1164
Reduced nicotinamide adenine dinucleotide	NADH	C00004	HMDB0001487	$C_{21}H_{29}N_7O_{14}P_2$	664.1175	666.1321
Nicotinamide adenine dinucleotide phosphate	$NADP^+$	C00006	HMDB0000217	$C_{21}H_{29}N_7O_{17}P_3$	742.0682	744.0827
Reduced nicotinamide adenine dinucleotide phosphate	NADPH	C00005	HMDB0000221	$C_{21}H_{30}N_7O_{17}P_3$	744.0838	746.0984
Nicotinamide		C00153	HMDB0001406	$C_6H_6N_2O$	121.0407	123.0553
ADP-ribose	ADPR	C00301	N/A	$C_{15}H_{23}N_5O_{14}P_2$	558.0644	560.0789
Cyclic ADP-ribose	cADPR	C13050	N/A	$C_{15}H_{21}N_5O_{13}P_2$	540.0538	542.0684
Lactate		C00186	HMDB0000190	$C_3H_6O_3$	89.0244	91.0390
2-hydroxyglutarate		C02630	HMDB0059655	$C_5H_8O_5$	147.0299	149.0445

Supplementary Figure Legends

Supplementary Fig. S1 | Rab4A targets CD4 to the lysosome in primary human CD4$^+$ T cells (n = 5). In Rab4A variant AAV-infected CD4$^+$ T cells from healthy donors (n = 5), Rab4A$^+$ CD4$^+$ T cells exhibit increased colocalization of CD4 and LysoTracker Red (LTR) compared to GFP vector control and Rab4A^{DN} cells. Statistical significance was assessed by one-way ANOVA with Tukey's correction for multiple comparisons. Data are presented as mean ± SEM.

Supplementary Fig. S2 | Rab4A promotes recycling of CD38 to the cell surface in CD4$^+$ T, CD8$^+$ T, and B cells. A CD38 recycling assay in immune cells isolated from B6 transgenic (TC) mouse splenocytes (n = 3 per genotype) shows **(A)** CD4$^+$ T cells enhanced CD38 surface recycling in B6.TC/Rab4A^{Q72L} mice compared to both B6.TC control and B6.TC/Rab4A^{Q72L}-KO mice, **(B)** CD8$^+$ T cells have significantly elevated recycling of CD38 to the cell surface in B6.TC/Rab4A^{Q72L} mice compared to B6.TC/Rab4A^{Q72L}-KO mice, **(C)** double negative (DN) T cells have no significant difference, **(D)** B cells have significantly elevated recycling of CD38 to the cell surface in B6.TC/Rab4A^{Q72L} mice compared to B6.TC/Rab4A^{Q72L}-KO mice, and **(E)** non-B and non-T cells have significantly lower recycling of CD38 to the cell surface in B6.TC/Rab4A^{Q72L} mice compared to B6.TC/Rab4A^{Q72L}-KO mice. Statistical significance was determined by two-way ANOVA. Error bars represent mean ± SEM.

Supplementary Fig. S3 | Rab4A promotes CD38 localization to the plasma membrane in Jurkat cells. (A) Western blots show isolation of plasma membrane, organelle membrane, nuclei, and cytosol fractions. As controls, all fractions contained actin, while cytosolic fraction only contained transaldolase, using whole cell extract as positive control (1,2). **(B)** Western blot (n = 6 independent cell culture repeats) shows that CD38 protein levels are significantly increased in the plasma membrane fraction of Rab4A$^+$ Jurkat cells compared to controls. Statistical significance was determined using two-way ANOVA with Tukey's correction for multiple comparisons. Data are presented as mean ± SEM.

Supplementary Fig. S4 | CD38 knockout in Rab4A-overexpressing Jurkat cells attenuates mTOR activation. (A) Western blot (n = 5 independent cell culture replicates) and **(B)** flow cytometry (n = 3-6 independent cell culture replicates, depending on cell line and stimulation conditions) confirm CRISPR-mediated CD38 knockout (CD38^{KO}) in control, Rab4A$^+$, and Rab4A^{DN} Jurkat cells. **(C-D)** Western blot and **(E-F)** flow cytometry reveal that CD38 knockout (CD38^{KO}) in Rab4A$^+$ Jurkat cells (n = 3 independent cell culture replicates) reduces phosphorylation of **(C, E)** 4E-BP1 and **(D, F)** AKT1. Statistical significance was determined by two-way ANOVA with Turkey's correction for **(A**) and Sidak's correction for **(B**) for multiple comparisons, **(C)** paired t-test, and **(D-F)** unpaired t-test. Data are presented as mean ± SEM.

Supplementary Fig. S5 | CD38 decreases TNFα, IFNγ, and IL-2 production in Rab4A AAV-transduced primary CD4$^+$, CD8$^+$, and DN T cells from healthy donors. Flow cytometry of Rab4 AAV-infected T cells from healthy donors shows that **(A)** the percentage of TNFα$^+$ IL-2$^+$ cells is significantly higher in CD38$^-$ cells compared to CD38$^+$ cells in CD4$^+$ T, CD8$^+$ T, and DN T cells. TNFα$^+$ IL-2$^-$ cells are significantly higher in CD38$^-$ cells compared to CD38$^+$ cells in Rab4A$^+$ CD4$^+$ T cells, in all AAV-infected CD8$^+$ T cells, and Rab4A$^+$ and Rab4A^{DN} DN T cells. The percentage of TNFα$^-$IL-2$^+$ cells is unchanged in CD4$^+$ and DN T cells. However, it is higher in CD38$^-$ cells compared to CD38$^+$ cells in GFP control vector-infected CD8$^+$ T cells. **(B)** The percentages of IFNγ$^+$ IL-2$^+$ and IFNγ$^+$ IL-2$^-$ cells are significantly higher in CD38$^-$ cells compared to CD38$^+$ cells in CD4$^+$ T, CD8$^+$ T, and DN T cells. The percentage of IFNγ$^-$ IL-2$^+$ cells is significantly higher in

$CD38^-$ cells compared to $CD38^+$ cells in $CD4^+$ T cells and GFP control vector AAV-infected $CD8^+$ T cells. **(C)** The percentage of $TNF\alpha^+$ $IFN\gamma^+$ cells is significantly higher in $CD38^-$ cells compared to $CD38^+$ cells in $CD4^+$ T, $CD8^+$ T, and DN T cells. The percentage of $TNF\alpha^+$ $IFN\gamma^-$ cells is significantly higher in $CD38^-$ cells compared to $CD38^+$ cells in $CD4^+$ T and $CD8^+$ T cells. The percentage of $TNF\alpha^-IFN\gamma^+$ cells is significantly higher in $CD38^-$ cells compared to $CD38^+$ cells in $CD4^+$ T and DN T cells. Statistical significance was determined by two-way ANOVA with Sidak's correction for multiple comparisons. Data are presented as mean ± SEM.

Supplementary Fig. S6 | Rab4A-mediated CD38 expression and IL-2 suppression occur independently of mTOR signaling. (A) Western blot shows that mTOR activation is inhibited with rapamycin treatment (n = 3 independent culture repeats). **(B)** Flow cytometry analysis shows that rapamycin significantly increases CD38 expression in $Rab4A^+$ Jurkat cells compared to DMSO vehicle control. In contrast, intracellular IL-2 levels are significantly reduced following rapamycin treatment compared to DMSO across all groups, suggesting that CD38-mediated IL-2 suppression is independent of mTOR signaling. Statistical significance was determined by two-way ANOVA with Sidak's correction for multiple comparisons. Data are presented as mean ± SEM. DOXY = doxycycline.

Supplementary Fig. S7 | Rab4A impairs NADPH-dependent kynurenine metabolism independently of CD38, resulting in kynurenine accumulation. (A-B) Targeted liquid chromatography tandem mass spectrometry (LC-MS/MS) analysis of Jurkat cells (n = 5 independent cell culture replicates) reveals that $Rab4A^+$ cells exhibit reduced levels of $NADP^+$ and NADPH compared to controls. CD38 knockout ($CD38^{KO}$) in $Rab4A^+$ cells does not restore these levels, indicating that Rab4A regulates $NADP^+$ metabolism independently of CD38. **(C)** Untargeted LC-MS/MS analysis shows that kynurenine levels are significantly increased in $Rab4A^+$ cells, and $CD38^{KO}$ in $Rab4A^+$ cells restores kynurenine levels. **(D)** NADPH is required for kynurenine-3-hydroxylase to convert kynurenine into 3-hydroxykynurenine, which is a precursor for NAD^+ synthesis. Statistical significance was determined by one-way ANOVA with Tukey's correction for multiple comparisons for comparing control, $Rab4A^+$, and $Rab4A^{DN}$ Jurkat cells and an unpaired t-test to compare $CD38^{WT}$ and $CD38^{KO}$ $Rab4A^+$ Jurkat cells**.** Data are presented as mean ± SEM.

Supplementary Fig. S8 | Rab4A increases nicotinamide levels in B6.TC mice. Sera from B6.TC/$Rab4A^{Q72L}$ mice have elevated nicotinamide levels compared to B6.TC mice. Upon 3-PEHPC treatment, nicotinamide levels significantly decrease in B6.TC/$Rab4A^{Q72L}$ mice compared to untreated. The number of mice in each genotype is as follows: B6.TC untreated (n = 15), B6.TC 3-PEHPC treated (n = 14), B6.TC/$Rab4A^{Q72L}$ untreated (n = 13), B6.TC/$Rab4A^{Q72L}$ 3-PEHPC treated, B6.TC/ $Rab4A^{Q72L}$-KO untreated (n = 7) and B6.TC/ $Rab4A^{Q72L}$-KO 3-PEHPC treated (n = 7). Statistical significance was determined by two-way ANOVA with Tukey's correction for multiple comparisons. Data are presented as mean ± SEM.

Supplementary Fig. S9 | Rab4A enhances glycolytic metabolism via CD38 and promotes 2-hydroxyglutarate accumulation through a CD38-independent pathway in Jurkat cells. Untargeted LC-MS/MS analysis of Jurkat cells (n = 5 independent cell culture replicates) shows that $Rab4A^+$ cells exhibit elevated levels of **(A)** lactate and **(B)** 2-hydroxyglutarate compared to controls. CD38 knockout ($CD38^{KO}$) in $Rab4A^+$ cells restores **(A)** lactate levels but not **(B)** 2-hydroxyglutarate levels. Statistical significance was determined by one-way ANOVA with Tukey's correction for multiple comparisons for comparing control, $Rab4A^+$, and $Rab4A^{DN}$ Jurkat cells and

an unpaired t-test to compare $CD38^{WT}$ and $CD38^{KO}$ $Rab4A^{+}$ Jurkat cells**.** Data are presented as mean ± SEM.

REFERENCES

1. Oaks, Z., A. Patel, N. Huang, G. Choudhary, T. Winans, T. Faludi, D. Krakko, M. Duarte, J. Lewis, M. Beckford, S. Blair, R. Kelly, S. K. Landas, F. A. Middleton, J. M. Asara, S. K. Chung, D. R. Fernandez, K. Banki, and A. Perl. 2023. Cytosolic aldose metabolism contributes to progression from cirrhosis to hepatocarcinogenesis. *Nat. Metab.* 5:41.

2. Winans, T., Z. Oaks, G. Choudhary, A. Patel, N. Huang, T. Faludi, D. Krakko, J. Nolan, J. Lewis, S. Blair, Z. Lai, S. K. Landas, F. Middleton, J. M. Asara, S. K. Chung, B. Wyman, P. Azadi, K. Banki, and A. Perl. 2023. mTOR-dependent loss of PON1 secretion and antiphospholipid autoantibody production underlie autoimmunity-mediated cirrhosis in transaldolase deficiency. *J. Autoimmun.* 140:103112.

Figure S1

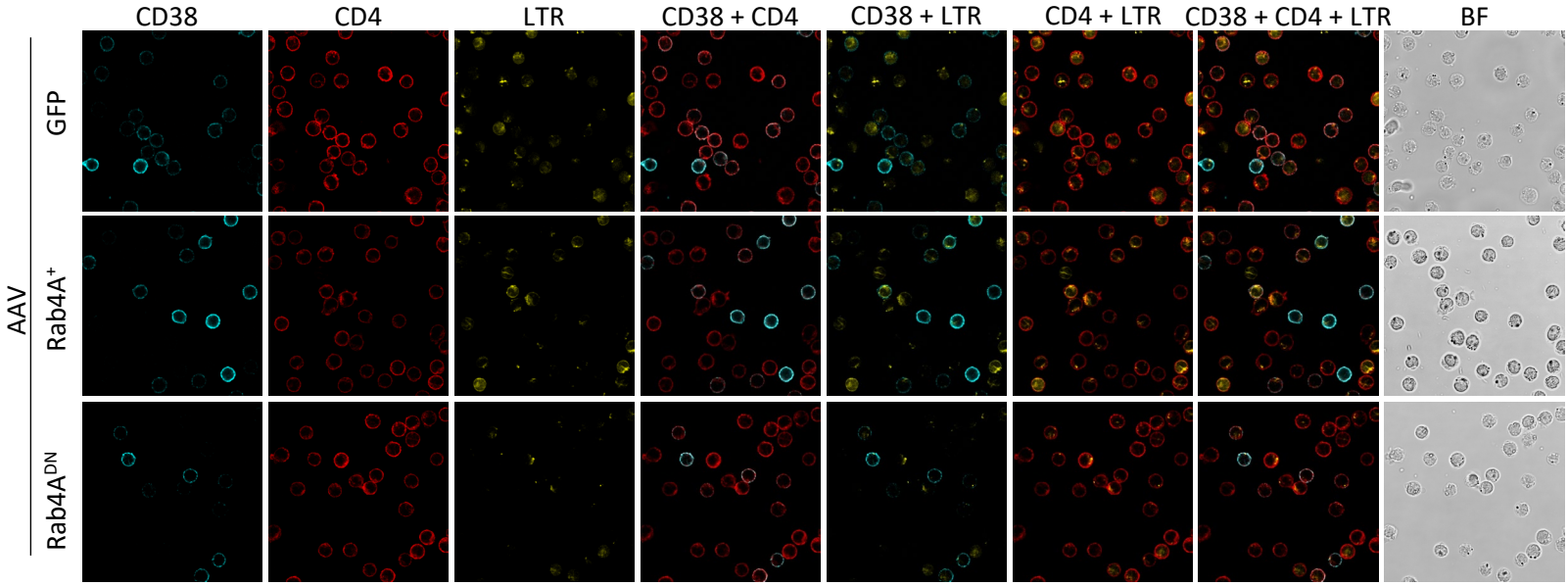
CD38
CD4
LTR
CD38 + CD4
CD38 + LTR
CD4 + LTR
CD38 + CD4 + LTR
BF
AAV
GFP
Rab4A+
Rab4ADN

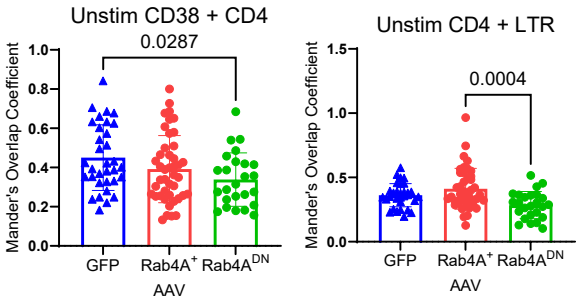
Unstim CD38 + CD4
0.0287
Mander's Overlap Coefficient
1.0
0.8
0.6
0.4
0.2
0.0
GFP
Rab4A+
Rab4ADN
AAV

Unstim CD4 + LTR
0.0004
Mander's Overlap Coefficient
1.5
1.0
0.5
0.0
GFP
Rab4A+
Rab4ADN
AAV

Figure S2

A

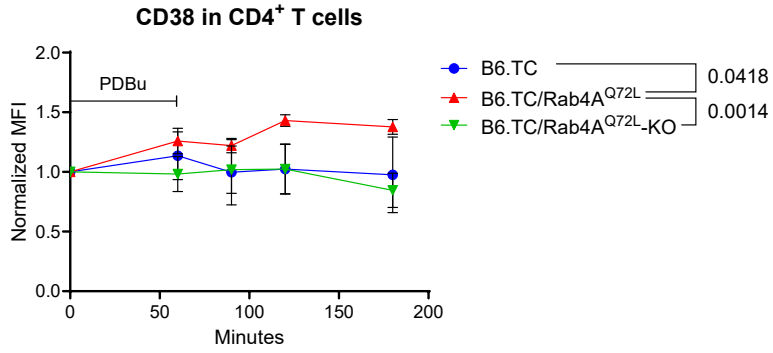

B

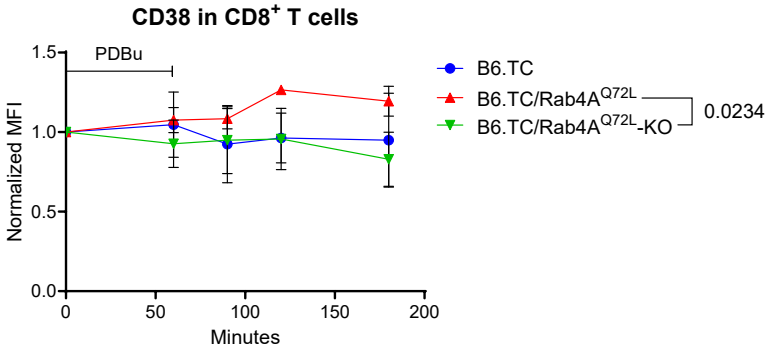

C

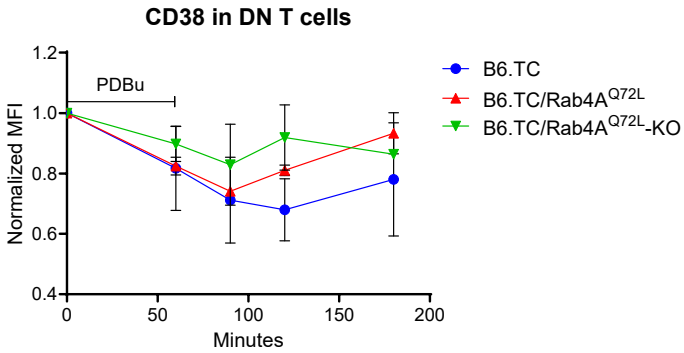

D

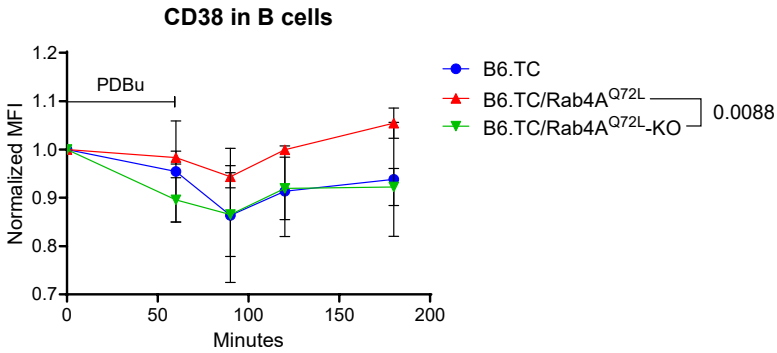

E

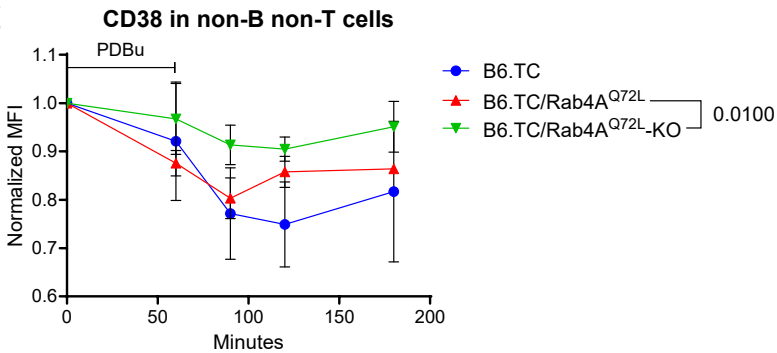

Figure S3

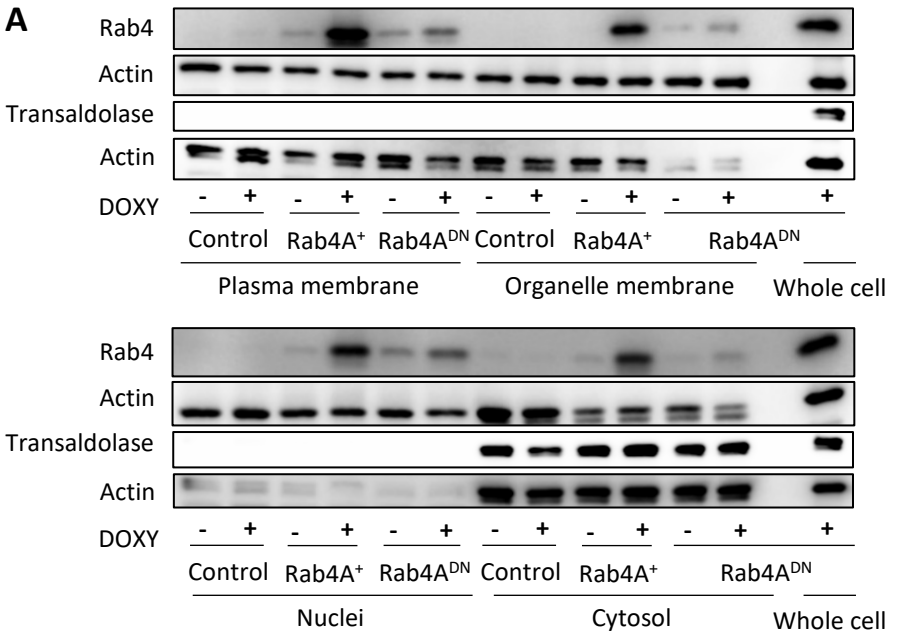
A
Rab4
Actin
Transaldolase
Actin
DOXY
- + - + - + - + - + - + +
Control
Rab4A+
Rab4ADN
Control
Rab4A+
Rab4ADN
Plasma membrane
Organelle membrane
Whole cell
Rab4
Actin
Transaldolase
Actin
DOXY
- + - + - + - + - + - + +
Control
Rab4A+
Rab4ADN
Control
Rab4A+
Rab4ADN
Nuclei
Cytosol
Whole cell

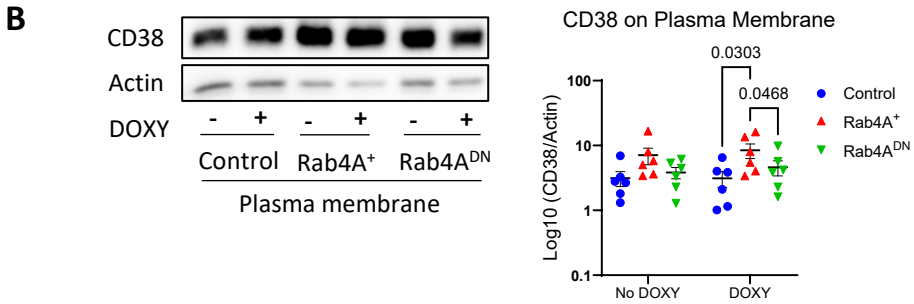
B
CD38
Actin
DOXY
- + - + - +
Control
Rab4A+
Rab4ADN
Plasma membrane
CD38 on Plasma Membrane
0.0303
0.0468
Control
Rab4A+
Rab4ADN
Log10 (CD38/Actin)
100
10
1
0.1
No DOXY
DOXY

Figure S4

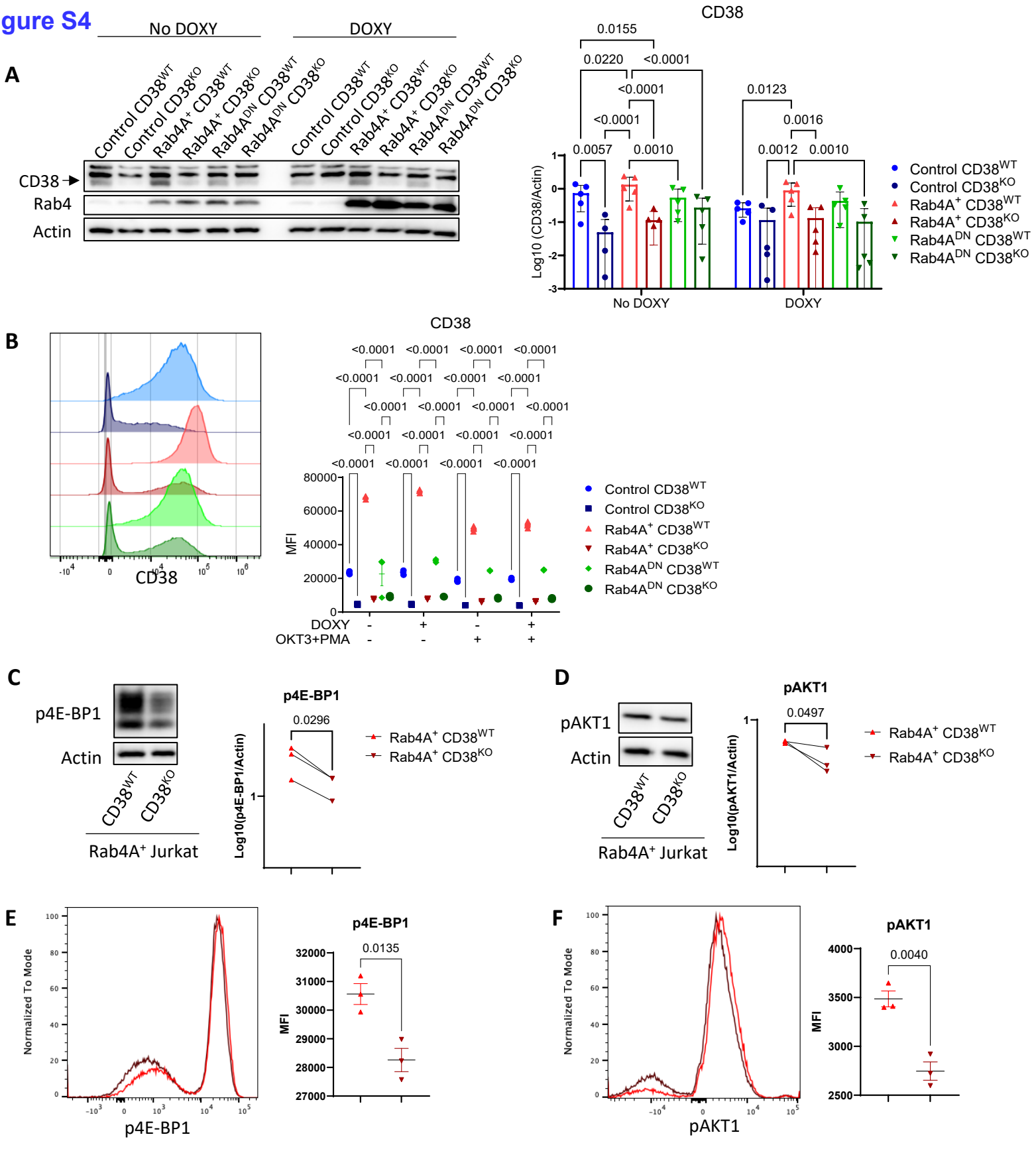
A
No DOXY
DOXY
Control CD38WT
Control CD38KO
Rab4A+ CD38WT
Rab4A+ CD38KO
Rab4ADN CD38WT
Rab4ADN CD38KO
CD38
Rab4
Actin
CD38
0.0155
0.0220
<0.0001
<0.0001
<0.0001
0.0123
0.0016
0.0057
0.0010
0.0012
0.0010
Log10 (CD38/Actin)
No DOXY
DOXY
B
CD38
<0.0001
MFI
DOXY
OKT3+PMA
C
p4E-BP1
Actin
CD38WT
CD38KO
Rab4A+ Jurkat
p4E-BP1
0.0296
Log10(p4E-BP1/Actin)
D
pAKT1
Actin
Rab4A+ Jurkat
pAKT1
0.0497
Log10(pAKT1/Actin)
E
Normalized To Mode
p4E-BP1
p4E-BP1
0.0135
MFI
F
Normalized To Mode
pAKT1
pAKT1
0.0040
MFI

Figure S5

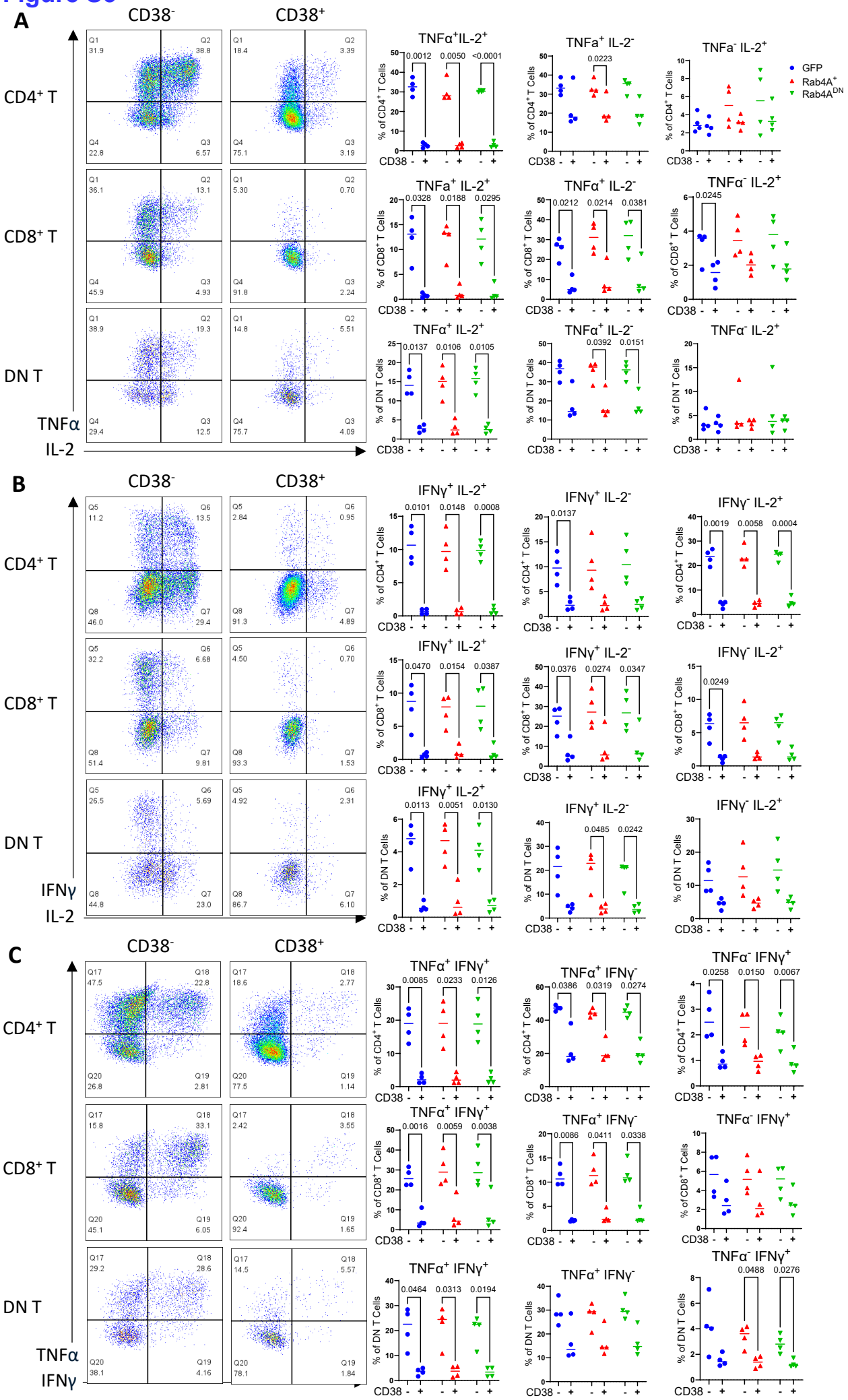
A
CD38-
CD38+
CD4+ T
CD8+ T
DN T
TNFα
IL-2
TNFα+IL-2+
TNFa+ IL-2-
TNFa- IL-2+
TNFα+ IL-2-
TNFα- IL-2+
GFP
Rab4A+
Rab4ADN
% of CD4+ T Cells
% of CD8+ T Cells
% of DN T Cells
CD38
B
IFNγ
IFNγ+ IL-2+
IFNγ+ IL-2-
IFNγ- IL-2+
C
TNFα+ IFNγ+
TNFα+ IFNγ-
TNFα- IFNγ+

Figure S6

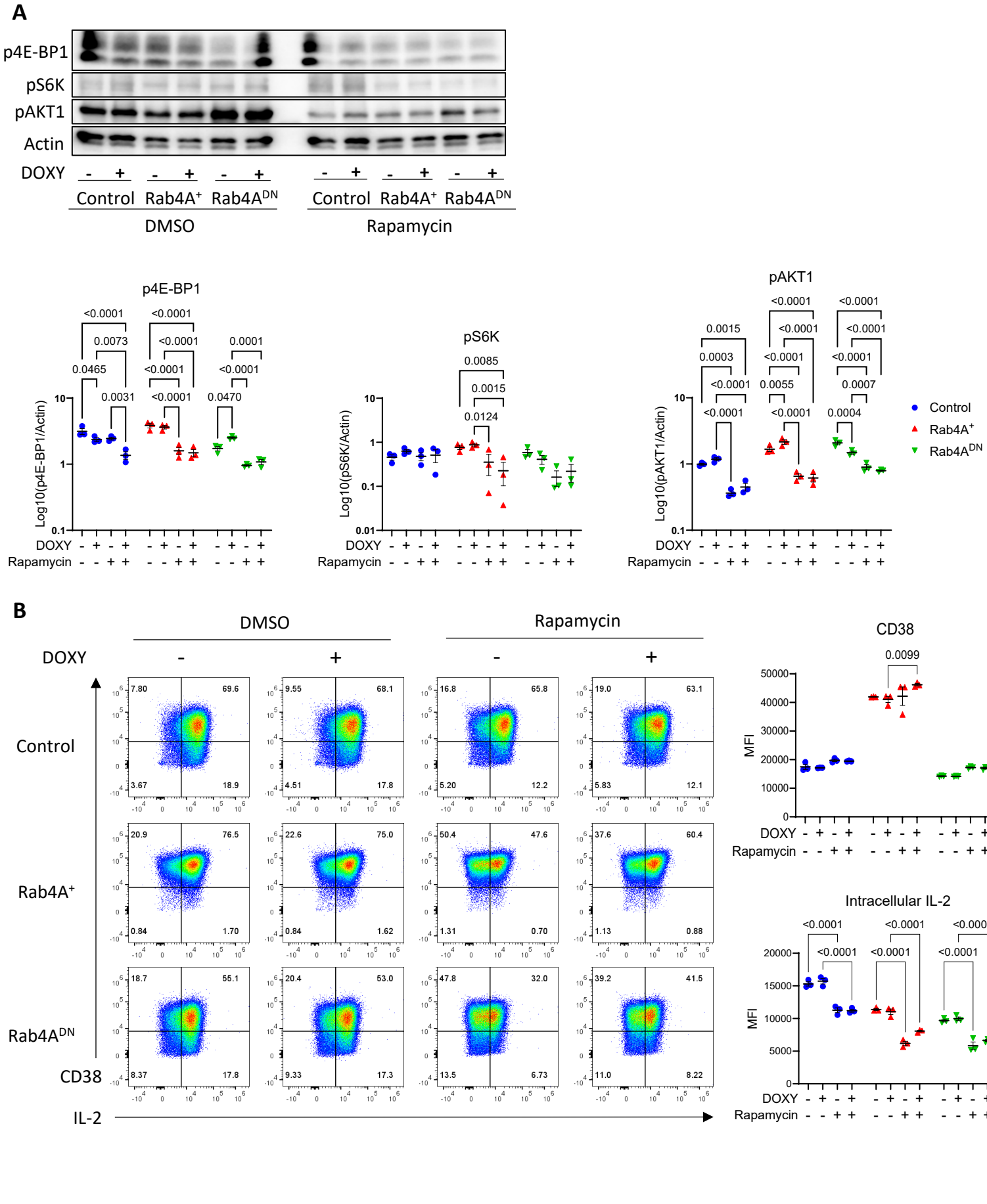
A
p4E-BP1
pS6K
pAKT1
Actin
DOXY
Control
Rab4A+
Rab4ADN
DMSO
Rapamycin
p4E-BP1
Log10(p4E-BP1/Actin)
pS6K
Log10(pS6K/Actin)
pAKT1
Log10(pAKT1/Actin)
Control
Rab4A+
Rab4ADN
B
DMSO
Rapamycin
Control
Rab4A+
Rab4ADN
CD38
IL-2
MFI
Intracellular IL-2

Figure S7

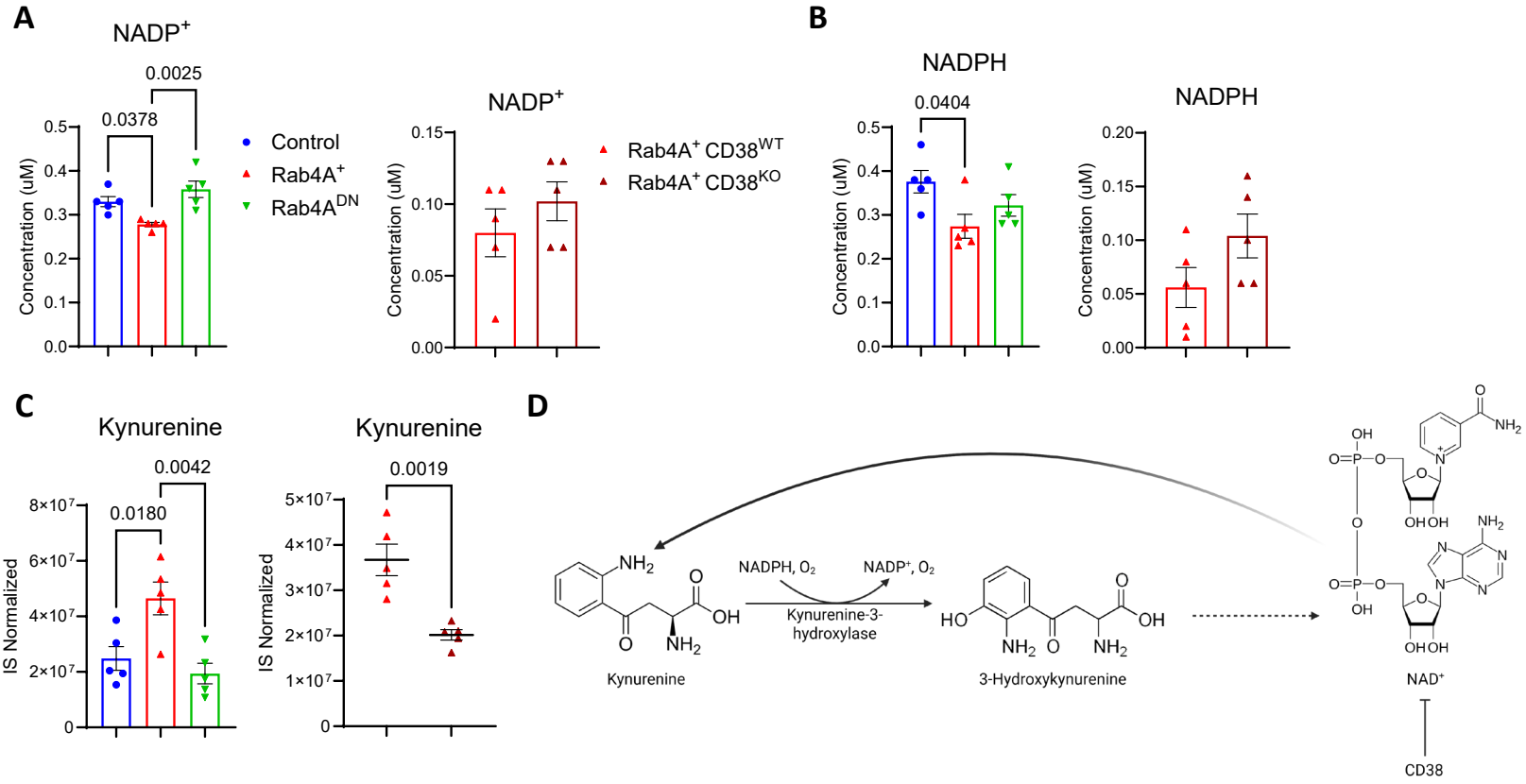
A
NADP+
0.0025
0.0378
Concentration (uM)
Control
Rab4A+
Rab4ADN
NADP+
Rab4A+ CD38WT
Rab4A+ CD38KO
B
NADPH
0.0404
NADPH
C
Kynurenine
0.0042
0.0180
IS Normalized
Kynurenine
0.0019
D
NADPH, O2
NADP+, O2
Kynurenine-3-hydroxylase
Kynurenine
3-Hydroxykynurenine
NAD+
CD38

Figure S8

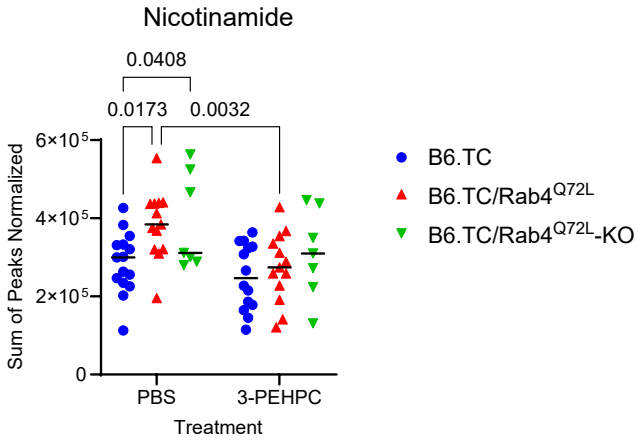
Nicotinamide
0.0408
0.0173
0.0032
6×10⁵
4×10⁵
2×10⁵
0
Sum of Peaks Normalized
PBS
3-PEHPC
Treatment
B6.TC
B6.TC/Rab4Q72L
B6.TC/Rab4Q72L-KO

Figure S9

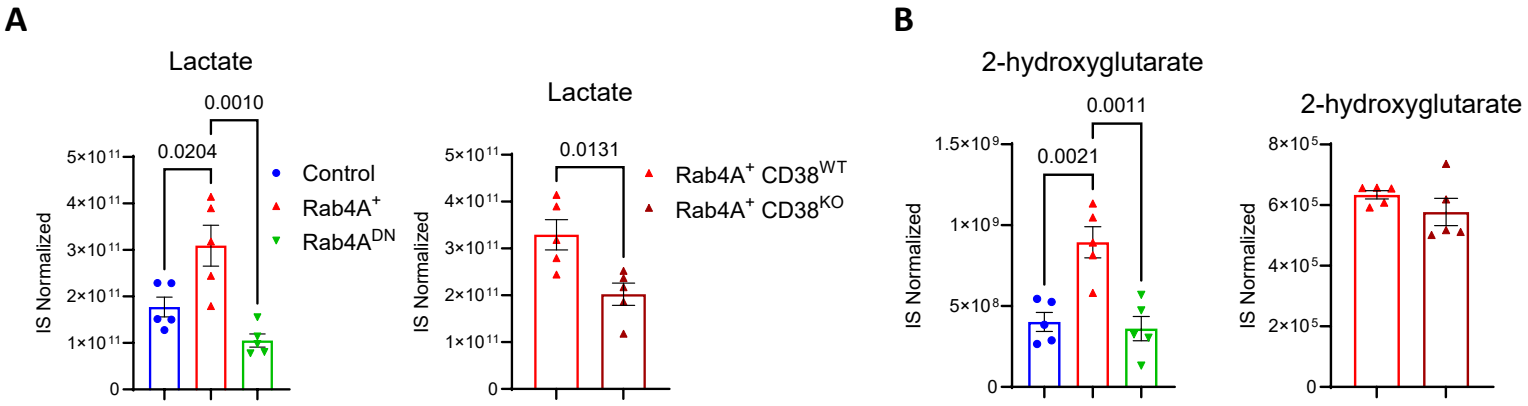
A
Lactate
0.0010
0.0204
5×10^11
4×10^11
3×10^11
2×10^11
1×10^11
0
IS Normalized
Control
Rab4A+
Rab4ADN
Lactate
0.0131
Rab4A+ CD38WT
Rab4A+ CD38KO
B
2-hydroxyglutarate
0.0011
0.0021
1.5×10^9
1×10^9
5×10^8
2-hydroxyglutarate
8×10^5
6×10^5
4×10^5
2×10^5

Graphical Abstract